Sensitivity of Point Defects in One Dimensional Nanocircuits

Steven R. Hunt, Phuc D. Hoang, Vaikunth R. Khalap, Danny Wan, Brad L. Corso, and Philip G. Collins
Department of Physics and Astronomy, University of California at Irvine, Irvine, CA USA 92697
collinsp@uci.edu

***Abstract*—When tailored to contain a single resistive defect, one dimensional nanocircuits can realize high dynamic range, high bandwidth transduction of single molecule chemical events. The physical mechanisms behind this sensitive transduction, however, remain poorly understood. Here, we complement ongoing sensing measurements with scanning probe characterization of the electronic properties of defects. The high sensitivity of defect sites is directly probed, and is found to be in excellent agreement with a finite element model containing realistic device parameters for the defect sites. The model illuminates the most likely sensing mechanisms of these single molecule circuits, and fully supports the premise that further tailoring of the defect sites could enable the chemically selective interrogation of a wide range of complex molecular interactions.**

I. Background and Motivation

Electronic devices formed from novel materials like nanowires, carbon nanotubes, or nanoclusters ("nanosensors") continue to be considered for many possible applications, but one of the most promising areas is in chemical sensing and detection. In this area, nanosensors generally have unequalled sensitivity and the promise of integrability with standard CMOS control systems. However, multiple technical issues have stalled the successful commercialization of such sensors.

An excellent example is the case of single walled carbon nanotubes (SWNTs), hollow molecular wires in which every conduction electron resides on the outer surface of the wire, in constant communication with the surrounding chemical environment. SWNTs are famously sensitive to virtually all environments, including air [1], water [2] and noble gases [3]. Thus, much of the work on SWNTs has focused on improving their selectivity and reducing unwanted responses. Furthermore, multiple physiochemical mechanisms lead to chemosensitivity in SWNT devices [4, 5]. For example, adsorbates can directly transfer charge to a SWNT, but also adsorb on nearby sites to which the SWNT is sensitive, such as oxide charge traps, interfacial Schottky barriers, and SWNT-SWNT junctions. The combination of possible interactions is daunting and remains under investigation on an analyte-by-analyte basis [5].

In addition to these problems, a more surprising shortcoming of SWNTs is their failure to provide high speed, high sensitivity response to analytes. SWNT sensors have relatively slow dynamics, even though a molecular device should in principle have single molecule sensitivity and the bandwidth to dynamically transduce chemical events: to directly interrogate single molecule attachments, charge transfer events, or other chemical dynamics, and to produce a rich, real-time data stream without ensemble averaging. In practice, the nanosensor literature, whether utilizing nanowires, nanoclusters, or SWNTs, typically depicts multi-second response times, even when the transduction is purported to result from few-molecule detection events. This particular discrepancy is not so consequential to commercial applications (i.e. to calibrated concentration responses), but it is a remarkable failing for electronic nanoscience. Relatively little progress has been achieved towards the nanotechnological limit of employing these nanosensors for dynamic, single-molecule sensing.

To address this failure, we have carefully considered the transduction mechanisms of nanosensor devices and attempted to amplify their sensitivity to single molecule events. Even a SWNT, as a nearly ballistic, molecular conductor, is an extended system ill-suited to discriminating individual events. Instead, a more ideal architecture concentrates the entire sensor response at a single active site in the device.

II. Single Site Molecular Sensors

To experimentally realize this model system, isolated point defects have been introduced into SWNT devices [6, 7]. The SWNT itself completes a three-terminal, field-effect device. When the defect site accounts for the majority of the device resistance and/or chemosensitivity, however, then the rest of the SWNT merely plays the role of interconnective wiring to the sensitized site.

Many factors contribute to the successful fabrication of effective SWNT transducers, and some of these are described previously in [6]. The use of single, clean, small diameter SWNTs grown in place by chemical vapor deposition is the preferred implementation. Passivation of the SWNT-metal contacts minimizes competing transduction at those interfaces. Metallic (m-) and semiconducting (s-) SWNTs are both effective at sensing when point defects are added, but the least ambiguous results come from m-SWNTs, which are not intrinsically sensitive to small changes in charge or local electric fields.

This work is supported by the NSF (DMR-0801271, CBET- 0729630, ECS-0802077, and CHE-0802913) and the NCI of the NIH (R01-CA133592-01).

The most important factor is found to be, not surprisingly, the chemical nature of the defect introduced into the SWNT. Our defects are introduced electrochemically with continuous electrical monitoring, providing the advantage that the same SWNT is characterized before, during and after modification [6]. Ether, phenol, epoxide, and other adduct groups are all found to increase the device resistance and introduce additional gate sensitivity to both m-SWNTs and s-SWNTs. These chemical groups are somewhat limited, however, for further derivatization. Further damage can be accumulated to introduce a carboxylic acid group [7]. Successful addition of a carboxylic group not only provides a more versatile chemical handle, but also increases the device resistance ten to one hundred fold, thereby accomplishing the primary goal of single site sensitization.

After fabrication, single site devices have been probed with various analytes. Exquisite sensitivity, including single molecule dynamic detection, has been demonstrated [8, 9]. In addition, the presence of a point defect has been clearly shown to amplify the chemosensitivity compared to pristine SWNT devices [10]. Examples of both cases of sensing are shown in Fig. 1. Despite successes fabricating and utilizing these single site sensors, though, a clear understanding of the mechanisms responsible has only begun to be investigated [11-13].

III. Sensing Mechanisms

A. *Local Probing of Defect Scattering*

To better understand the response of SWNT defects, and devices based upon them, a theoretical model of the devices has been constructed and tested against experimental data. Critical to this testing is the use of conductive tip atomic force microscopy (AFM) techniques to map out tfhe local electronic properties of devices. Kelvin probe microscopy (KFM) is used to directly measure the electric potentials around a SWNT defect, and scanning gate microscopy (SGM) is used to measure the degree of gate sensitivity close to and far from a defect site. Both techniques are useful, but this report focuses exclusively on the latter to probe the behavior of defect sites.

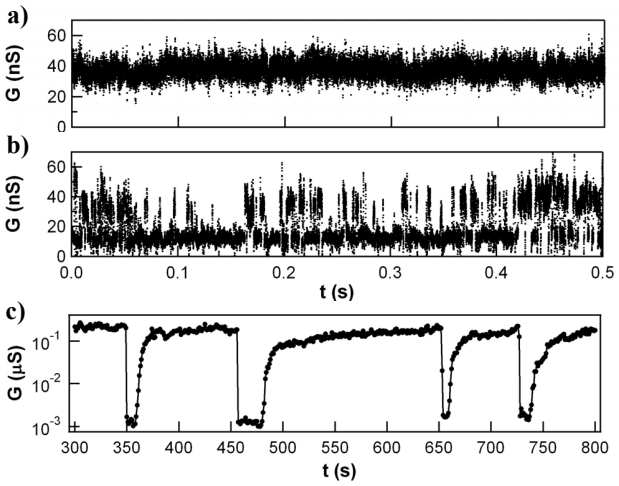

Figure 1. Chemical sensing by point defect SWNT devices. (a,b) A SWNT with a carboxylic defect is monitored versus time in 20 mM phosphate buffer solution before (a) and after (b) the addition of 10 μM N-ethyl-N'-(3-dimethylaminopropyl) carbodiimide hydrochloride (EDC). EDC is a reagent that selectively attaches to carboxyl groups, resulting in the added fluctuations observed in (b). (c) Pd-decorated SWNTs exhibit sensing responses of 30-60% when probed with H_2 gas, but when the same measurement is performed with a Pd-decorated defect, the response is approximately one hundred fold. Experiments are fully described in [8-10].

Fig. 2 illustrates the general principle of the measurements and the particular advantage of SWNT point defects. The device architecture is portrayed in Fig. 2a with a cartoon of a protein sensing element attached to a SWNT device at its defect site. The SGM measurement technique is depicted in Fig. 2b. SGM involves monitoring changes in device conductivity *G* between the source and drain electrodes that results from interactions between the device channel and the biased cantilever. In our case, the channel is the SWNT and the tip can probe inhomogeneities along it. An SGM image, which is usually acquired simultaneously with surface topography, directly images the positions at which *G* is sensitive to perturbing fields, and it has proven particularly useful for imaging SWNT defect sites [6, 14]. Fig. 2 shows the topography (Fig. 2c) and SGM image (Fig. 2e) of a m-SWNT containing a defect, produced by point oxidation in water. This example clearly demonstrates the ideal case of a single position being sensitive to local gating. A similarly treated s-SWNT is shown in Figs. 2d,f. Due to the semiconducting band structure, the s-SWNT also has a sensitive Schottky barrier that is visible in the SGM image at the electrode interface.

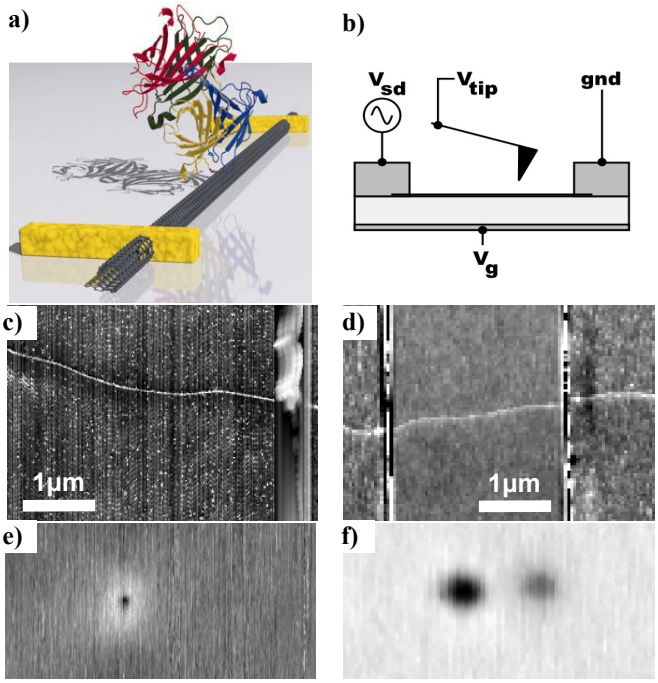

Figure 2. (a) Conceptual device, in which a protein or other sensing molecule is covalently attached to a SWNT defect site. (b) Schematic of the SGM and SGS techniques, in which device sensitivity is probed locally using a conductive AFM cantilever biased at V_{tip}. (c) AFM topography image and (d) simultaneous SGM image for a m-SWNT containing a phenolic defect from point oxidation in water. (e,f) Identical sequence for a similarly-treated s-SWNT, in which both a defect and a Schottky barrier respond to gating.

These SGM examples support the working hypothesis for the mechanism of single site sensing, which is that any chemical interaction involving charge transfer, charged species, or charge dipoles adsorbing on the SWNT might be sensitively transduced into G fluctuations. In a device dominated by a single site, the resulting G signal might be generated by single molecule, rather than ensemble, responses.

Despite the apparent simplicity of this model and the compelling SGM images in Fig. 2, the situation is known to be more complex. SGM images are highly dependent on bias and other imaging conditions, even when isolated features can be imaged [15-20]. In addition, electrostatic hysteresis can make some SGM features difficult to reproduce. As a specific example, five SGM images from the same SWNT defect site are shown in Fig. 3. In this s-SWNT example, the backgate bias V_g is varied from -9V to -7V, changing the band bending and carrier concentration at the Schottky barrier. Minority carrier injection through a Schottky barrier at the bottom of each image dominates the SGM sensitivity at V_g = -9.0 or -8.5 V. A defect site in the center of each image alternates between being gate sensitive (at V_g = -8.0 V) and insensitive (V_g = -7.0 V). The images illustrate not only the effects of strong V_g dependence, but also a possibly uncorrelated relationship between the two barriers. Thus, while SGM is useful for identifying and counting defect sites, and even for estimating their sensitivity, the technique is clearly limited. Quantitative analysis of defect scattering and defect sensitivity requires much more precise control than shown in Fig. 3.

B. Scanning Gate Spectroscopy

To improve upon the conventional measurement, we have implemented a voltage sweeping SGM technique that captures the entire bias dependence at positions along a SWNT. Whereas standard SGM images map the conductance change $\Delta G(x,y)$ as a function of surface position, a sweep of either the cantilever tip bias V_{tip} or backgate bias V_g at each position allows us to determine the full function $\Delta G(V_{tip},V_g,x,y)$. With knowledge of the relevant capacitances, these biases determine the potential and energy of a SWNT site, turning the SGM technique into a form of electrostatic spectroscopy. Our technique relies on a high vacuum AFM with a liquid nitrogen cold finger (JEOL JSPM-5200), controlled by a custom LabVIEW application. The cryogenic capability greatly improves reproducibility by minimizing hysteretic, electrostatic surface effects that can eliminate contrast in conventional SGM.

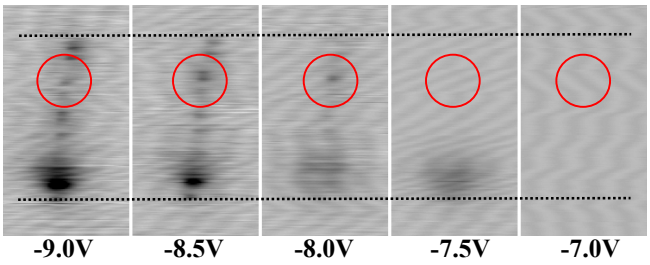

Figure 3. SGM images taken at different backgate voltages V_g as labelled. Circles highlight the same SWNT location in each image, while dotted lines show approximate source and drain electrode positions. All images share the same greyscale, representing ΔG = 0% (white) to 75% (black).

The resulting advantage of SGM spectroscopy, or simply scanning gate spectroscopy (SGS), is demonstrated in Fig. 4 for two different s-SWNTs containing defects. In these images, the x-axis extends from before the source electrode to the drain, and the y-axis represents the changing gating condition. Fig. 4a shows an example of the V_g sweep method. At most positions, the turn-on threshold in the presence of the tip is at V_g = -6 V. When the AFM tip approaches the defect centered at x = 1.9 µm, the threshold dips steeply to -9 V. An SGM image at V_g = -8 V would appear very similar to Fig. 2e, but here the SGS image displays the entire bias dependence.

Fig. 4c shows the V_{tip} sweep method of measuring $\Delta G(V_{tip}, x)$ on another s-SWNT. The biases here are chosen to directly compare the defect region, centered at x = 3.0 µm, to modulation of the Schottky barrier. The band edge in this case is at a higher potential outside of the measurement range.

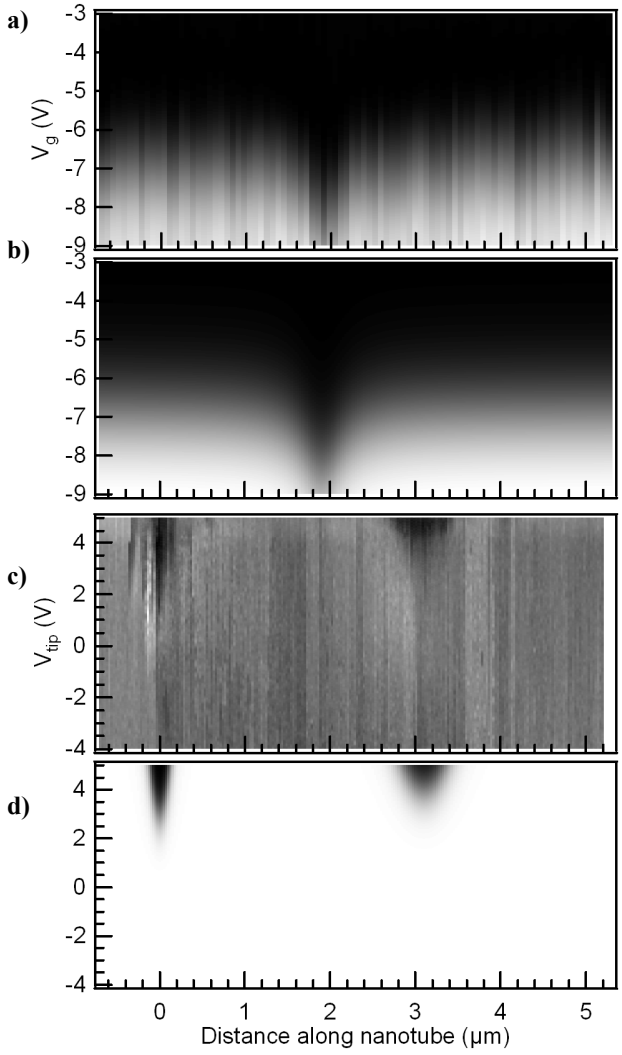

Figure 4. (a,c) Scanning gate spectroscopy images acquired along two s-SWNTs containing defects. Depending on the imaging mode, the y-axis can be V_g (a) or V_{tip} (c). (b,d) Corresponding SGS simulations resulting from the model described in Section III-D. Images and models share the same scale, representing ΔG = 0% (white) to 100% (black).

The SGS images provide a fine-grained, more complete depiction of each defect's electrostatics, and the apparent vertical and horizontal width of the defect features can be directly converted into meaningful physical parameters. From the spatial extent of the affected region, we extract a tip-defect capacitance, assuming that the defect itself is only weakly coupled to the SWNT carriers. From the vertical offset ΔV_{tip} = 1 V between the Schottky barrier and the defect in Fig. 4c, we directly measure the height of the defect barrier relative to the flat-band condition of the Schottky barrier. By using the measured tip-defect capacitance and calculated tip-backgate capacitance, this potential difference can be directly converted into an energy difference of approximately 200 meV.

C. *Modelling the Defect Electrostatics*

Further quantitative analysis of the experimental data requires a specific model of the defect's electronic structure. A simple tunneling barrier disrupting the SWNT bandstructure is found to be sufficient to reproduce most SGS data sets, even though more complete transport spectroscopy suggests the presence of internal degrees of freedom [21]. We constructed a finite element device model for a single-defect, three-terminal SWNT device by defining a region of width a_b in which the density of states is gapped to simulate the absence of low energy, extended states. The system is modeled in COMSOL with an electrolyte gate surrounding the SWNT in order to approximate the true conditions of the sensing measurements. For simplicity, the SWNT length is reduced to 100 nm and the defect is centered at x = 50 nm. Titanium source and drain electrodes are included, and all potentials are referenced to 0 V at the source electrode.

Fig. 5 shows the result of solving the full electrostatics of a system with a m-SWNT device in electrolyte and determining the potentials everywhere along the SWNT as a function of the applied V_g. For clarity of presentation, we consider the case of a wide barrier a_b = 10 nm, and no source-drain potential difference. Because of its high conductivity and strong equilibration with the electrodes, the potential of the m-SWNT is only weakly affected by gating. Instead, its potential is nearly fixed at 0.17 V by the Ti-carbon work function difference. The defect region, on the other hand, is capacitively coupled to both the electrolyte and the rest of the system, with a ratio that determines its intermediate potential.

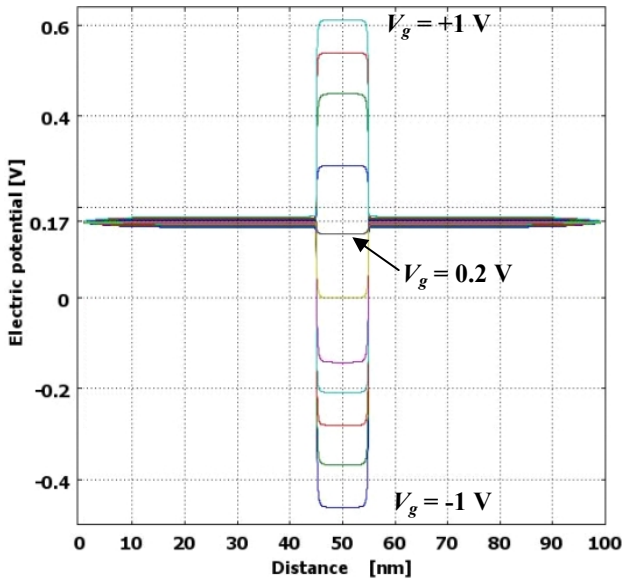

Figure 5. Model of the local electrostatic potential along a 100 nm segment of m-SWNT, evaluated versus electrolyte gate bias, $-1 < V_g < 1$ V. The defect site is much more responsive to gating than the pristine m-SWNT, and this difference in sensitivity results in either an attractive or repulsive barrier to SWNT carriers. Near V_g = 0.2 V, the defect becomes nearly transparent.

Fig. 5 clearly contrasts the effectiveness of gating on the defect barrier compared to along the SWNT. For $V_g > 0.4$ V, the defect becomes a high, repulsive barrier (to electron-like carriers) that can substantially reduce the device conductance G. At $V_g > 0$ V, however, the defect is an attractive well that can modulate G non-monotonically depending on the number of bound states and resonances. A flat band condition occurs near V_g = 0.26 V at which the defect barrier is aligned with the SWNT band. When gated at this condition, the barrier becomes substantially transparent.

Even though the model shown in Fig. 5 is for an electrolytic gate, it is very relevant to the experimental measurements. Especially for the case of insensitive m-SWNTs, local gating of the defect site by V_{tip} in SGS measurements proceeds in much the same way. Devices with semiconducting band structures have been studied and are slightly more complex: they follow the same trends but with greater modulation of the local s-SWNT bands by V_{tip}, matching those observed in Fig. 4a. The lack of a simple, analytical expression for the one-dimensional Schottky barrier hampers accurate modeling of cases like Fig. 4c.

D. *Modelling the Defect Transmission and Sensitivity*

To extend the model further, defect barrier heights E_b are determined as a function of the relevant gating conditions. Tunneling transmission probabilities are then calculated for the actual barrier height and shape within the WKB approximation. Parameterization of the results determines a curve of $T_{defect}(V_g)$, the transmission probability of a defect as a function of the gating potential(s). The Landauer-Buttiker formalism then directly relates $T_{defect}(V_g)$ to relative conductance changes in one-dimensional devices [22].

Using this process, it is straightforward to use the finite element model to simulate SGS images for defects in both s-SWNTs and m-SWNTs. Example simulations are shown in Figs. 4b and 4d, directly below the corresponding experimental data. Excellent qualitative agreement can be obtained, even for devices with multiple barriers having different a_b and E_b fitting parameters.

In fact, the SGS technique makes meaningful, quantitative comparisons particularly straightforward. A vertical line cut taken through an SGS image is a direct measurement of $G(V_{tip})$, the conductance observed during local gating of a region by the tip. When the tip is located over a defect site, the SWNT bandstructure and Schottky barriers (if present) are relatively unperturbed, allowing the remainder of the device to be represented by a single, constant transmission coefficient T_{bulk} in series with T_{defect}. By assigning the maximum value of

$G(V_{tip})$ to the transparent defect state $T_{defect} = 1$, T_{bulk} is determined and the function $T_{defect}(V_{tip})$ directly results from

$$G(V_{tip}) = (4e^2/h)\,[1/T_{bulk} + 1/T_{defect} - 1]^{-1}. \qquad (1)$$

An example of this quantitative comparison of experiment and theory is illustrated in Fig. 6. $G(V_{tip})$ data taken from an SGS image is converted into $T_{defect}(V_{tip})$ and then fitted to the model transmission using a_b and E_b as fitting parameters (Fig. 6b). For this device, excellent agreement is found with values a_b = 0.3 nm and E_b = 0.13 eV [23], values which are physically quite reasonable for carbon lattice defects [24]. Excellent agreement between the calculation and the experimental conductance measurements indicates that the model, while simple, provides a reasonable estimation of the defect's transport properties.

Even more importantly, the agreement indicates a direct connection not only between the model and the SGS data, but also with the typical sensing behaviors portrayed in Fig. 1. The extreme sensitivity of the single site devices is in complete agreement with the barrier height modulation observed in Fig. 5. Discrete charges as small as ±e at the defect site are sufficient to change the relative barrier height. Because the tunneling transmission is exponentially dependent on this barrier height, device conductance transduces small changes to the barrier with enormous amplification. It is noteworthy that the same amplification allows for the stabilization of tunneling microscopes, with the microscope's vacuum tunneling gap playing the role of the SWNT defect site in this discussion.

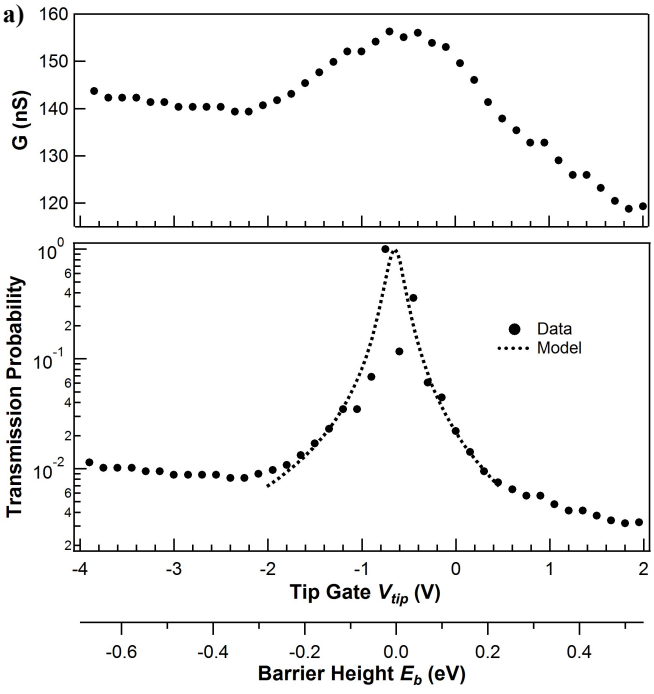

Figure 6. Vertical linecut of $G(V_{tip})$ from an SGS image. The raw data (a) is converted into a defect transmission probability (b) using Eq. 1 and measurements of the device resistance before the defect is added. The model transmission in (b) is the WKB tunneling probability for the corresponding barrier heights derived from the finite element model. Adapted from [23].

IV. Conclusions

Chemical sensing by defect sites in one dimensional devices is a promising route towards high bandwidth circuits with single molecule sensitivity. In this report, such circuits are probed directly with scanning gate microscopy and a variant, scanning gate spectroscopy, to interrogate the sensing mechanisms. By acquiring the entire bias dependence of local gating, it becomes straightforward to compare experiments to a simple model in which a defect site is electrostatically gated.

Excellent agreement between the data and model provides a direct connection between the scanning probe data and the typical sensing behaviors shown in Fig. 1. Furthermore, the modeling establishes the mechanism of single-site sensing to be primarily electrostatic. The resistance of single site devices varies exponentially with the tunneling probability at the defect site, making these devices exceedingly sensitive to perturbative charges or fields in the surrounding environment.

Acknowledgment

We acknowledge helpful discussions with B.R. Goldsmith, J.G. Coroneus, and G.A. Weiss, and the technical assistance of A.M. Chan and S.M. Denning.

References

[1] P. G. Collins, K. Bradley, M. Ishigami, and A. Zettl, "Extreme oxygen sensitivity of electronic properties of carbon nanotubes," Science, vol. 287, pp. 1801-1804, Mar 10 2000.

[2] H. E. Romero, G. U. Sumanasekera, S. Kishore, and P. C. Eklund, "Effects of adsorption of alcohol and water on the electrical transport of carbon nanotube bundles," Journal of Physics-Condensed Matter, vol. 16, pp. 1939-1949, Mar 31 2004.

[3] H. E. Romero, K. Bolton, A. Rosen, and P. C. Eklund, "Atom Collision-Induced Resistivity of Carbon Nanotubes," Science, vol. 307, pp. 89-92, Jan 7 2005.

[4] I. Heller, A. M. Janssens, J. Mannik, E. D. Minot, S. G. Lemay, and C. Dekker, "Identifying the mechanism of biosensing with carbon nanotube transistors," Nano Letters, vol. 8, pp. 591-595, 2008.

[5] K.-J. Lee and J. Kong, "Chemical Sensing with SWNT-FETs," in Carbon Nanotube Electronics, A. Javey and J. Kong, Eds. New York: Springer, 2009.

[6] B. R. Goldsmith, J. G. Coroneus, V. R. Khalap, A. A. Kane, G. A. Weiss, and P. G. Collins, "Conductance-controlled point functionalization of single-walled carbon nanotubes," Science, vol. 315, pp. 77-81, 5 Jan 2007.

[7] J. G. Coroneus, B. R. Goldsmith, J. A. Lamboy, A. A. Kane, P. G. Collins, and G. A. Weiss, "Mechanism-Guided Improvements to the Single Molecule Oxidation of Carbon Nanotube Sidewalls," ChemPhysChem, vol. 9, pp. 1053-6, 2008.

[8] B. R. Goldsmith, J. G. Coroneus, A. A. Kane, G. A. Weiss, and P. G. Collins, "Monitoring single molecule reactivity on a carbon nanotube," Nano Letters, vol. 8, pp. 189-194, 2008.

[9] B. R. Goldsmith, J. G. Coroneus, J. Lamboy, G. A. Weiss, and P. G. Collins, "Scaffolding Carbon Nanotubes into Single-Molecule Circuitry," Journal of Materials Research, vol. 23, pp. 1197-1201, May 2008.

[10] V. R. Khalap, T. Sheps, A. A. Kane, and P. G. Collins, "Hydrogen Sensing and Sensitivity of Palladium-Decorated Single-Walled Carbon Nanotubes with Defects," Nano Letters, vol. 10, pp. 896-901, Feb. 15 2010.

[11] L. M. Zhang and M. M. Fogler, "Scanned gate microscopy of a one-dimensional quantum dot," Nano Letters, vol. 6, pp. 2206 - 2210, 2006.

[12] L. Prisbrey, G. Schneider, and E. Minot, "Modeling the Electrostatic Signature of Single Enzyme Activity," Journal of Physical Chemistry B, vol. 114, pp. 3330-3333, Mar 11 2010.

[13] Y. Kanai, V. R. Khalap, P. G. Collins, and J. C. Grossman, "Atomistic Oxidation of a Carbon Nanotube in Nitric Acid," Physical Review Letters, vol. 104, p. 066401, 2010.

[14] Y. Fan, B. R. Goldsmith, and P. G. Collins, "Identifying and counting point defects in carbon nanotubes," Nature Materials, vol. 4, pp. 906-911, 2005.

[15] A. Bachtold, M. S. Fuhrer, S. Plyasunov, M. Forero, E. H. Anderson, A. Zettl, and P. L. McEuen, "Scanned probe microscopy of electronic transport in carbon nanotubes," Phys. Rev. Lett., vol. 84, pp. 6082-6085, Jun 26 2000.

[16] M. T. Woodside and P. L. McEuen, "Scanned probe imaging of single-electron charge states in nanotube quantum dots," Science, vol. V296, pp. 1098-1101, 2002.

[17] C. Staii and A. T. Johnson, "High frequency scanning gate microscopy and local memory effect of carbon nanotube transistors," Nano Letters, vol. 5, pp. 893-896, 2005.

[18] C. Staii, A. T. Johnson, and N. J. Pinto, "Quantitative analysis of scanning conductance microscopy," Nano Letters, vol. 4, pp. 859-862, 2004.

[19] Y. Kim, Y. M. Oh, J. Y. Park, and S. J. Kahng, "Mapping potential landscapes of semiconducting carbon nanotubes with scanning gate microscopy," Nanotechnology, vol. 18, Nov 2007.

[20] M. Freitag, J. C. Tsang, A. Bol, P. Avouris, D. N. Yuan, and J. Liu, "Scanning photovoltage microscopy of potential modulations in carbon nanotubes," Applied Physics Letters, vol. 91, 2007.

[21] J. Mannik, B. R. Goldsmith, A. Kane, and P. G. Collins, "Chemically induced conductance switching in carbon nanotube circuits," Phys. Rev. Lett., vol. 97, p. 16601, 2006.

[22] S. Datta, Electronic Transport in Mesoscopic Systems. Cambridge: Cambridge University Press, 1995.

[23] S. R. Hunt, B. L. Corso, D. Wan, and P. G. Collins, "Scanning Gate Spectroscopy and its Application to Carbon Nanotube Defects," in press.

[24] P. G. Collins, "Defects and disorder in carbon nanotubes," in Oxford Handbook of Nanoscience and Technology: Frontiers and Advances, A. V. Narlikar and Y. Y. Fu, Eds. Oxford: Oxford Univ. Press, 2010.